Available online at www.sciencedirect.com
ScienceDirect
Geochimica et Cosmochimica Acta 74 (2010) 3539–3552
Geochimica et Cosmochimica Acta
www.elsevier.com/locate/gca

Interfacial energy effects and the evolution of pore size distributions during quartz precipitation in sandstone

Simon Emmanuel [a,*,1], Jay J. Ague [a], Olav Walderhaug [b]

[a] Department of Geology and Geophysics, Yale University, P.O. Box 208109, New Haven, CT 06520-8109, USA
[b] Statoil ASA, N-4035 Stavanger, Norway

Received 16 November 2009; accepted in revised form 15 March 2010; available online 23 March 2010

Abstract

Pore size is usually thought to control the rate of crystal growth in porous geological media by determining the ratio of mineral surface area to fluid volume. However, theory suggests that in micron-scale to nanometer scale pores, interfacial energy (surface energy) effects can also become important. Interfacial energy typically increases the solubility of very small crystals growing in tiny pores, and when the fluid is close to equilibrium – as is often the case in geological systems – mineral precipitation could occur in relatively large pores, while in very small adjacent pores crystal growth might be suppressed. Such a mechanism would effectively restrict the reactive surface area of the porous medium, thereby reducing the bulk reaction rate. We investigated the pore size distributions in naturally cemented sandstone adjacent to an isolated stylolite and found that quartz precipitation was inhibited in pores smaller than 10 μm in diameter. Furthermore, we demonstrate that kinetic formulations which assume constant solubility cannot reproduce the observed pore size patterns in mineralized samples; by contrast, excellent fits with the data are obtained when interfacial energy effects are taken into account. Reaction rates in geological media determined in field studies can be orders of magnitude lower than those measured in laboratory experiments, and we propose that reduced reaction rates in porous media with micron and submicron-scale porosity could account for much of the apparent paradox.

1. INTRODUCTION

Porosity is one of the fundamental parameters that determines the way in which fluids behave in rock and soil. However, porosity in natural porous media often comprises pores of many different sizes, and this distribution of pore sizes can strongly influence permeability, specific surface area, and acoustic properties of the porous matrix (e.g., Bear, 1972; Uchida, 1987; Bryant, 1995). Thus, understanding the factors controlling the evolution of pore size distributions has important implications for a host of geological settings that involve changing porosity, such as carbon sequestration in geological formations, hydrocarbon extraction from subsurface reservoirs, and diagenesis in sedimentary basins.

One of the main mechanisms for altering porosity and pore size distributions is mineral precipitation. While the effect that mineralization has on total porosity has been studied extensively, its influence on pore size distributions is less well documented. Even though overall porosity is reduced by mineral precipitation, secondary porosity can form between growing crystals (Fig. 1), and the formation of "honeycomb" cement can even create bimodal pore size distributions (Sullivan and McBride, 1991). In other instances the precipitating mineral may coat existing grains in continuous overgrowths (e.g., Walderhaug and Bjørkum, 2003; Zhu, 2005). While such phenomena are commonly observed in rocks, the quantification of their effect on pore size distributions and an understanding of the rates at which they occur has been limited.

* Corresponding author. Tel.: +972 2 6586875; fax: +972 2 5662581.
E-mail address: simonem@cc.huji.ac.il (S. Emmanuel).
[1] Present address: Institute of Earth Sciences, The Hebrew University of Jerusalem, Edmond J. Safra Campus, Givat Ram, Jerusalem 91904, Israel.

0016-7037/$ - see front matter © 2010 Elsevier Ltd. All rights reserved.
doi:10.1016/j.gca.2010.03.019

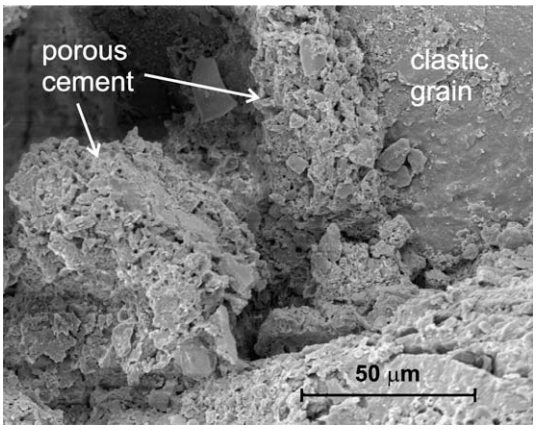

Fig. 1. SEM image of porous "honeycomb" cement between clastic grains in Frio sandstone, Texas.

Pore size is generally thought to influence the rates of mineral dissolution and precipitation in rock and soil by directly controlling the surface area available for reaction: the ratio of surface area to volume increases with decreasing pore size, and it is, therefore, expected that, all else being equal, mineral reactions that depend on mineral surfaces will proceed more rapidly as pores become smaller. However, in small nanometer to micron-scale pores, additional size related mechanisms could also influence reaction rates. For small particles, interfacial energy can play a critical role in determining the stability and solubility of solid phases (Adamson, 1990; Stumm and Morgan, 1996; McHale et al., 1997; Wettlaufer, 1999; Navrotsky et al., 2008). In the case of solubility, as crystal size decreases, interfacial energy effects typically cause crystals to dissolve more readily. Importantly for mineralization, when crystals grow within pores, crystal size may ultimately be limited by the dimensions of the voids, and consequently the effective solubility of a mineral phase should be inversely proportional to pore size (Scherer, 2004; Rijniers et al., 2005; Emmanuel and Berkowitz, 2007). Such effects of surface energy are expected to have a significant impact on bulk reaction kinetics in systems in which the concentration of the dissolved mineral phase is close to equilibrium; in such cases, the fluid phase may be oversaturated in large pores and undersaturated in small pores (Putnis et al., 1995; Emmanuel and Berkowitz, 2007), leading to a reduction in the overall rate of mineral precipitation.

As geochemical reactions often occur at conditions that are near local equilibrium and many rock types contain high levels of micron and submicron-scale porosity, geological systems can offer an excellent natural laboratory to study the role of pore size in controlling mineral kinetics. Indeed, some observations suggest that interfacial energy effects can act to suppress mineral precipitation in small pores: in one study of a halite-cemented sandstone, submicron-scale pores were found to remain open, while larger pores had been filled with cement (Putnis and Mauthe, 2001). Although such data provided qualitative evidence for the inhibition of mineralization in very small pores, a quantitative test of the mechanism was not carried out.

Mineralization in rocks and soils often involves two stages: (i) transport of a dissolved mineral phase through a porous matrix and (ii) subsequent precipitation of a mineral in the pore space. When mineralization proceeds in such a manner, gradients in porosity can develop, and systems that have evolved under such conditions should provide useful insight into the effect of mineral precipitation on the porous matrix. Moreover, it has recently been suggested that an examination of the pore size distributions of such mineralized rocks could help elucidate the effect of interfacial energy on mineralization in porous systems and test the limits of reactive transport models that predict pore size evolution (Emmanuel and Ague, 2009).

In this paper, we present a high-resolution profile of pore size distributions from a sandstone section adjacent to an isolated stylolite exhibiting spatially systematic changes in porosity due to varying levels of mineralization. The measurements are compared with a reactive transport model that takes into account surface energy effects and simulates the evolution of porosity and pore size distributions. The objective of this combined approach is to assess the performance of standard frameworks used to describe pore chemical kinetics in porous media and quantify the impact of interfacial energy on mineralization. We discuss the implications of our results for reaction rates in porous geological systems.

2. METHODOLOGY

2.1. Field data and analyses

Although mineralization is a ubiquitous process in geological media, the source of the precipitating mineral phase is often unconstrained, which can significantly impair efforts to understand the mechanisms controlling the evolution of the porous matrix. However, one diagenetic process that can create a well defined source for the dissolved phase is stylolite formation. Stylolites are irregular fracture-like features in rock that form where mineral grains, such as quartz and calcite, are dissolved along the contacts with clay-rich or micaceous laminae (Fig. 2). Crucially for the study of mineralization, much of the dissolved mineral phase often precipitates in the porous matrix (Mapstone, 1975; Wong and Oldershaw, 1981; Oelkers et al., 1996; Walderhaug and Bjørkum, 2003), and spatial gradients in porosity can develop. As the source of the mineralizing phase is known, well constrained models can be constructed to describe the evolution of the porous domain, and in particular the evolution of pore size distributions (e.g., Emmanuel and Ague, 2009).

However, for a comparison between measurements and model simulations to be meaningful, a stylolite-bearing rock must possess porosity gradients due to decreasing cementation away from the dissolution interface; samples with different porosities serve to demonstrate the effect of varying degrees of cementation on pore size distributions and help to constrain model parameters. While stylolites are a common feature of many sedimentary rocks, they are normally too closely spaced to allow the study of varying levels of cementation on the pore system.

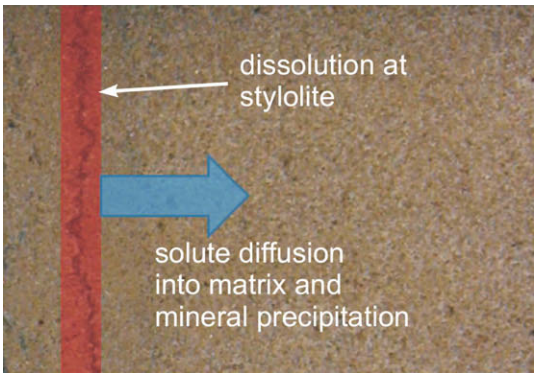

Fig. 2. Schematic representation of mineralization in stylolite-bearing rocks and associated porosity reduction. Dissolution is restricted to the stylolite interface (the irregular dark line in the red shaded region); the dissolved phase constantly diffuses into the porous matrix where it precipitates and reduces porosity. (For interpretation of the references to colour in this figure legend, the reader is referred to the web version of this article.)

One location in which significant porosity gradients have been reported in association with stylolites is the Stø Formation in the Barents Sea (Walderhaug and Bjørkum, 2003). Drill cores indicate that the Lower Jurassic formation is 84 m thick and comprises mainly very fine-grained to medium-grained shallow marine quartz sandstones; stylolite spacing in the formation is unusually large, often exceeding several meters. The top of the Stø Formation corresponds to 2049 m below the sea floor, with samples in the present study being taken from a depth of 2109 m below the sea floor. The reported current temperature in the formation is around 84 °C, although it may have reached 125 °C during previous deeper burial. A more detailed geological description of the formation is given elsewhere (Walderhaug and Bjørkum, 2003).

To characterize the pore size distributions as a function of distance, a 25 cm section of the core, adjacent to a stylolite, was sampled at 12 points. All the samples bar one represent a 1 cm thick slice of the core; to obtain a higher resolution in the region closest to the stylolite a single 0.5 cm slice was also taken. Total porosity, pore size distributions, and surface areas were measured by mercury injection porosimetry (Micromeritics AutoPore IV 9500 porosimeter; Micromeritics Analytical Services), a common technique used to characterize reservoir rock and sandstone (e.g., Uchida, 1987). Washburn theory (Washburn, 1921) is used to relate the intrusion pressure to the volume of mercury and hence reconstruct pore size distributions. Here, the results are reported for pores with diameters >10 nm. While mercury porosimetry possesses a number of limitations (e.g., the method often measures the largest entrance to a pore rather than the actual pore diameter), it remains a useful way of obtaining quantitative data that can be used to compare the pore structure of different samples. A more detailed account of the technique is given by Giesche (2006). To supplement the porosimetry data, high-resolution electron imaging was carried out using field-emission gun equipment at Yale University. Backscattered electron (BSE) images of polished samples were obtained using a JEOL JXA-8530F electron microprobe, whereas scanning electron microscope (SEM) work was performed on unpolished samples with a Philips XL-30 environmental SEM.

2.2. Conceptual models and numerical scheme

2.2.1. Kinetic models and pore size effects

One of the primary objectives of the study is to test the limits of standard kinetic theory when applied to mineral precipitation in porous media under geological conditions. Here, we describe the standard kinetic framework and discuss how it may be expanded to include the effects of precipitation in porous media comprising pores that range in size from nanometers to millimeters.

In standard kinetic theory, the reactive surface area of a porous material is one of the most important parameters in determining the rate of crystal growth (Berner, 1980; Lasaga, 1998). As the ratio of surface area to volume increases with decreasing pore size, it is usually expected that, for a given porosity, reactions, such as dissolution and precipitation, will accelerate as pores become smaller. In near-equilibrium porous systems, the bulk precipitation rate, Q, is typically given as (Lasaga, 1998)

$$Q = KA(S/S_0 - 1)^{\beta}, \tag{1}$$

where K is a kinetic rate coefficient, A is the specific reactive surface area, S is the ion activity product, S_0 is bulk solubility, and β is the rate order.

However, in small nanometer to micron-scale pores, surface energy strongly influences solubility, and it has recently been suggested that such effects can be accounted for by modifying existing kinetic models: when the porous medium comprises pores of uniform size, Eq. (1) becomes (Emmanuel and Ague, 2009)

$$Q = KA(S/S_d - 1)^{\beta}, \tag{2}$$

where S_d is the solubility in pores of size d determined by interfacial energy effects. Thus, in a porous medium containing small pores mineral solubilities should be higher and precipitation rates lower than in a porous medium with large pores.

It is important to note that the expressions for reaction rates given in Eqs. (1) and (2) are strictly speaking only applicable to unimodal pore size distributions. Rocks and soils, however, usually possess a wide range of pore sizes, and the rate associated with a given pore size d, Q_d, can be defined such that

$$Q_d = KA_d\left(\frac{S}{S_0} - 1\right)^{\beta} \tag{3}$$

if solubility is independent of pore size, or

$$Q_d = KA_d\left(\frac{S}{S_d} - 1\right)^{\beta} \tag{4}$$

if pore size influences the effective solubility. In both cases, A_d is the area associated with pores of size d, related to the total specific surface area by

$$A = \int_0^{\infty} A_d d(d), \tag{5}$$

and the overall reaction rate is given by

$$Q = \int_0^\infty Q_d d(d); \tag{6}$$

by substitution, the total rate is therefore defined as

$$Q = K \int_0^\infty A_d (S/S_d - 1)^\beta d(d). \tag{7}$$

Importantly for the purposes of this study, such definitions of partial reaction rates can be justified when reaction rates are slow relative to solute diffusion (Kang et al., 2003; Tartakovsky et al., 2007; Emmanuel and Ague, 2009), which is often the case in geological systems. We note, however, that testing such kinetic expressions in laboratory experiments remains the focus of ongoing work.

Treating the overall rate as the sum of different components can have non-trivial implications for the kinetics of geochemical reactions. While interfacial energy effects in micron-scale voids are not usually expected to produce an increase in solubility greater than 1% (Emmanuel and Ague, 2009), the impact on overall reaction rates may nevertheless be significant when systems (i) are very close to equilibrium and (ii) possess a high proportion of micron – nanometer scale pores. When such conditions prevail, models predict that crystal growth may simultaneously occur in large pores while being completely inhibited in small ones (Emmanuel and Berkowitz, 2007; Emmanuel and Ague, 2009), and the total rate of mineral precipitation in the porous medium should be much lower than expected due to the loss of reactive surface area associated with the small pores.

We emphasize here that most kinetic models assume that pore size has a minimal effect, and the treatment of polymodal pore size distributions and interfacial energy effects in small pores remains a non-standard approach; clearly though, to predict the evolution of pore size distributions in complex natural systems, a polymodal model is necessary. In the present study, we compare the performance of the constant solubility kinetic model (Eq. (3)) with that of the pore size dependent solubility model (Eq. (4)).

2.2.2. Model representations of the porous medium

Although previous models have used simple geometrical relations to predict the evolution of a unimodal pore size distribution during mineralization (e.g., Lasaga and Rye, 1993), only a limited number of studies have attempted to model the evolution of a spectrum of pore sizes (e.g., Emmanuel and Ague, 2009). Here, we adopt a continuum approach for the porous matrix in which the porosity comprises voids with a range of sizes; each discrete pore size, defined by the dimension d (Fig. 3), is assigned a partial porosity, ϕ_d, which is related to the total porosity, ϕ, by the expression

$$\phi = \int_0^\infty \phi_d d(d). \tag{8}$$

The pore space is represented as a bundle of interconnected tubes of various sizes such that the partial porosity associated with each pore size d can be defined as

$$\phi_d = X_d L_d, \tag{9}$$

where X_d is the cross sectional area of a pore of size d and L_d is the total length of d-sized pores per unit volume. For square cuboid-shaped pores of dimension d (Fig. 3), the cross sectional area of the individual pores is defined as (Emmanuel and Ague, 2009)

$$X_d = d^2 \left(1 - \frac{\omega - \sin\omega\cos\omega}{\sin^2\omega}\right), \tag{10}$$

where $\omega = (\pi/2 - \theta)/2$ (Fig. 3); in addition, the partial specific surface associated with each pore size is given by

$$A_d = \frac{4 L_d \omega d}{\sin\omega}. \tag{11}$$

We note that the precise geometry of the pores is not critical to model behavior: employing tubes with different cross sections has only a minor effect on the evolution of porosity.

In this treatment, we assume that no new nuclei are created during mineral precipitation and that crystal growth takes place only on pre-existing grain surfaces. While such an assumption is not appropriate for all types of mineralization, examination of the sandstone in the present study reveals that the precipitation occurs as overgrowths on pre-existing grains, and individual small crystals – which would presumably be present if new nucleation sites had formed – were not observed.

2.2.3. Bulk and effective solubilities in the porous domain

During stylolitization in sandstone, the primary mineral reaction can be summarized as

$$SiO_2(\text{quartz}) + 2H_2O \rightleftharpoons H_4SiO_4, \tag{12}$$

such that the bulk solubility, S_0, of quartz is defined by

$$S_0 = \frac{a^{eq}_{H_4SiO_4}}{(a_w)^2}, \tag{13}$$

where $a^{eq}_{H_4SiO_4}$ and a_w indicate the equilibrium activities of orthosilicic acid and water, respectively.

While the bulk solubility may be accurate for large crystals, micron and nanometer scale crystals can have much larger solubilities. This effect is related to the change in interfacial energy during crystal growth and the effective solubility, S_d, can be given by (Adamson, 1990: Scherer, 2004)

$$S_d = S_0 \exp\left(\frac{v_m \gamma \zeta}{RT}\right), \tag{14}$$

where v_m is the molar volume of the mineral, γ is the interfacial energy, R is the gas constant, and T is temperature. In addition, ζ represents the crystal curvature, defined as the rate of change of volume with respect to surface area; thus for a spherical crystal possessing a radius of curvature r_c, $\zeta = 2/r_c$ and Eq. (14) becomes

$$S_d = S_0 \exp\left(\frac{2 v_m \gamma}{RT r_c}\right). \tag{15}$$

A similar approach can be applied to the solubility of minerals growing within the pores of a porous medium. In this case, however, unlike crystals growing freely in solution, the maximum radius of curvature for crystals confined within rigid pores becomes a function of the pore size and is no longer equivalent to the radius of the crystal. For a crys-

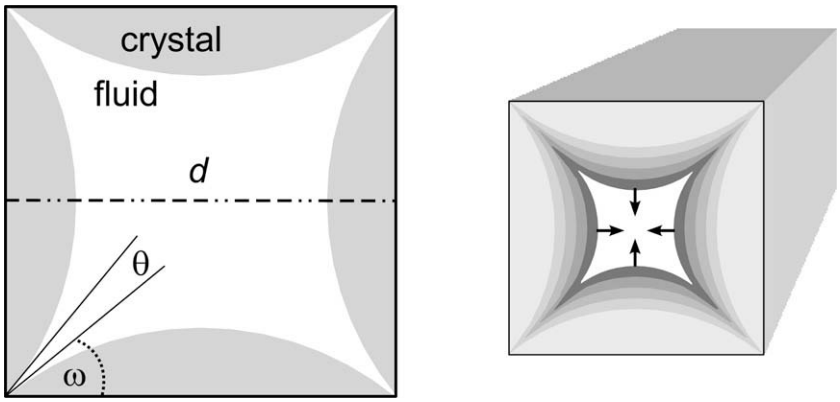

Fig. 3. Schematic diagram showing the geometry for the simulated crystal growth. Crystal growth is perpendicular to the walls of a square cuboid-shaped pore; as the pore is filled during mineralization, the pore size decreases, leading to an increase in crystal curvature and a corresponding increase in solubility. The dihedral angle corresponds to θ and the characteristic size of the pore is given by the dimension d. The arrows indicate the direction of crystal growth. Adapted from (Emmanuel and Ague, 2009).

tal growing in a cylindrical pore (Fig. 3), the radius of curvature is related to the radius of the pore, d, by $r_c = d/\cos\theta$, where θ is the dihedral angle. Substituting this relationship into Eq. (15) yields (Scherer, 2004)

$$S_d = S_0 \exp\left(\frac{2v_m\gamma\cos\theta}{RTd}\right); \tag{16}$$

as $\omega = (\pi/2 - \theta)/2$, the effective solubility can also be expressed as (Emmanuel and Ague, 2009)

$$S_d = S_0 \exp\left(\frac{4v_m\gamma\sin\omega}{RTd}\right). \tag{17}$$

Inserting typical parameter values into Eq. (17) reveals that the ratio S_d/S_0 can be significantly larger than unity in microscopic crystals. Importantly, crystals growing in voids typically possess convex rather than concave surfaces so that $\theta < \pi/2$ and $S_d > S_0$ for most cases (Scherer, 2004). Although concave surfaces may occur in microfractures, their effect is not considered in the present model.

In this paper we will differentiate between two measures of supersaturation: (i) the bulk supersaturation index, S/S_0 and (ii) the effective supersaturation index S/S_e; in both these expressions S refers to the ion activity product. The bulk supersaturation index is the standard measure for supersaturation and is independent of pore size; by contrast, the effective supersaturation index can vary from pore to pore depending on the interfacial energy effect.

2.2.4. Reactive transport equations

The model we employ here represents a standard diffusion-reaction equation for porous media; however, in addition to calculating changes to total porosity, the model simultaneously tracks the evolution of different pore sizes. The model assumes that at a given distance from the stylolite, solute concentrations are the same in all pores, irrespective of size; thus, the bulk supersaturation will not vary from pore to pore, while the effective saturation will change with pore size. Such an approach should be valid in systems close to equilibrium (Kang et al., 2006) – as is the case in the current study – and facilitates a continuum treatment of the problem. The series of dimensionless equations that describe mineral precipitation, solute diffusion, and the evolution of the porous matrix during stylolitization are summarized here, and an in-depth discussion is given in previous work (Emmanuel and Ague, 2009).

The non-dimensional reactive transport equation is given by

$$\frac{\partial(\phi\overline{C})}{\partial\bar{t}} = \frac{1}{Pe}\frac{\partial\left(\phi\frac{\partial\overline{C}}{\partial\bar{x}}\right)}{\partial\bar{x}} - \overline{Q}, \tag{18}$$

where ϕ is total porosity, $\overline{C}$ is the dimensionless H_4SiO_4 concentration (defined as $\overline{C} = C/S_0$, where C is the dimensional concentration), $\bar{t}$ is dimensionless time ($\bar{t} = tv/H$, where t is dimensional time, v is the velocity at which the stylolite boundary recedes due to dissolution, and H is the initial size of the domain), and $\bar{x}$ is the dimensionless distance (related to the dimensional distance, x, by $\bar{x} = x/H$). In addition, Pe is the Peclet number (given by $Pe = vH/D_e$), and $\overline{Q}$ is the dimensionless kinetic reaction. We note that in the definition of the Peclet number, the effective diffusion coefficient D_e is defined as $D_e = D_w/\tau$, where D_w is the free water diffusion coefficient and τ is tortuosity; porosity, which is usually included in D_e, instead appears in the product $\phi\frac{\partial\overline{C}}{\partial\bar{x}}$ in Eq. (18) so as to minimize the dependence of D_e on porosity.

In the model, the position of the dissolution front is expressed as $\bar{h} = 1 - \bar{t}$, and the boundary conditions for the equation become

$$\left.\frac{\partial\overline{C}}{\partial\bar{x}}\right|_{\bar{x}=1-\bar{t}} = 0 \tag{19}$$

and

$$\overline{J}|_{\bar{x}=0} = \frac{1-\phi}{S_0 v_m}. \tag{20}$$

The evolution of partial porosity is determined by

$$\frac{\partial\phi_d}{\partial\bar{t}} = -S_0 v_m \overline{Q}_d, \tag{21}$$

where

$$\overline{Q}_d = \overline{A}_d\kappa\left(\frac{S}{S_0} - 1\right)^{\beta} \tag{22}$$

for the constant solubility model and

$$\overline{Q}_d = \overline{A}_d \kappa \left(\frac{S}{S_d} - 1 \right)^{\beta} \tag{23}$$

for the pore size dependent solubility (interfacial energy) model. In this formulation, the non-dimensional partial specific surface area is defined as $\overline{A}_d = A_d H$, while the dimensionless rate coefficient is related to the equivalent dimensional parameter, K, by $\kappa = K/vS_0$. Thus, κ is a measure of the rate of mineral precipitation relative to the rate of stylolite dissolution. The total rate term in Eq. (18) is given by $\overline{Q} = \int_0^{\infty} \overline{Q}_d d(d)$.

For a given initial domain size and set of boundary conditions, the two non-dimensional parameters, Pe and κ, control the evolution of porosity in the system: the Peclet number regulates both the rate at which the stylolite interface recedes as well as the flux of dissolved material into the porous domain, while the non-dimensional rate coefficient determines the rate at which mineralization occurs. For geological systems, Pe is expected to fall in the range 10^{-9}–10^{-2}, while κ is estimated to vary from 10^0 to 10^9 (Emmanuel and Ague, 2009).

The moving boundary problem, which arises due to dissolution at the stylolite, can be dealt with by transforming the coordinate system to a domain of constant size. For further details of this technique and how it is applied specifically to the equations described in this section, the reader is referred to Emmanuel and Ague (2009).

2.2.5. Numerical methods

The series of coupled equations describing solute transport and porosity evolution are solved numerically using the COMSOL Multiphysics® software package based on finite elements. The numerical scheme employs a mesh comprising 3840 Lagrange quadratic elements and a time dependent linear system solver; higher mesh densities did not significantly affect the results.

The numerical model determines the evolution of porosity in a porous domain with an initially uniform porosity and polymodal pore size distribution; the porosity is binned into 16 different pore sizes in the range 10^{-7}–10^{-4} m to produce a cumulative porosity curve that matches that measured in the sample farthest from the stylolite interface (24–25 cm); this sample is least affected by mineralization and therefore, most likely to represent the state of the porous matrix prior to stylolitization. We note that Walderhaug and Bjørkum (2003) observed a small degree of "background" quartz cement (~5%) present in the Stø Formation at relatively large distances from the stylolites. For simplicity, we have assumed this quartz cement to have been precipitated uniformly prior to the beginning of stylolitization by localized diagenetic processes. Additional parameter values used in the simulations are given in Table 1.

To optimize the numerical model to the measured pore size distribution curves, an error minimization technique was employed which compared model solutions with the field data. An objective function, defined as the sum of the errors between the measured and predicted values, was minimized using a MATLAB algorithm based on the Nelder-Mead method. The method evaluates a function at the vertices of a simplex (the generalization of a tetrahedral region of space to arbitrary dimension), and then performs a sequence of transformations aimed at shrinking the simplex, until a predefined bound is reached. By fixing the initial domain size at 0.25 m, the technique yields optimal values for Pe, κ, and the duration of stylolitization. We emphasize here that we chose not to vary any of the parameters in Eq. (17) to obtain better fits for the interfacial energy model; values for γ, v_m, ω, and T are estimated from literature values (Table 1) and kept constant throughout the simulations.

Importantly for the interpretation of the results, it must be remembered that the model generates non-unique solutions i.e., different combinations of Pe, κ, and duration of stylolitization can produce similar pore size distribution patterns. Thus, although the optimal values for the model parameters must be treated as estimates only, the model can be used effectively to test the overall impact of interfacial energy on pore size distribution patterns.

Table 1
List of symbols and parameter values.

Symbol	Definition	SI Units	Value
H	Initial domain size	m	0.25
S_0	Quartz solubility product	mol m^{-3}	0.1995[a]
T	Temperature	K	357[b]
a_w	Seawater activity		0.98[a]
β	Empirical rate order		1
γ	Interfacial free energy	J m^{-2}	0.35[a,c]
θ	Dihedral angle		$\pi/4$[d]
v_m	Molar volume	m^3 mol^{-1}	2.269×10^{-5}[e]

[a] Stumm and Morgan (1996).
[b] Current temperature in the Stø Formation, although quartz may have precipitated at higher temperatures (Walderhaug and Bjørkum, 2003).
[c] Parks (1984).
[d] Emmanuel and Ague (2009).
[e] Lide (1996).

3. RESULTS

3.1. Measured pore size distributions

Consistent with previous reports of porosity in the Stø Formation (Walderhaug and Bjørkum, 2003), our measurements indicate that total porosity changes sharply in the region directly adjacent to the stylolite, increasing from 12.1% at a distance of 0–0.5 cm to 20.9% at 3–4 cm (Fig. 4); beyond this zone, the porosity appears to fluctuate slightly around an average value of approximately 20%, probably reflecting a degree of heterogeneity in the porosity prior to mineralization. The overall porosity pattern demonstrates that mineralization associated with stylolitization occurs primarily in the region directly adjacent to the dissolution interface, with the rock matrix farthest from the stylolite undergoing far less change.

Inspection of BSE images of polished samples (Fig. 5) reveals that porosity is much lower near the stylolite interface, with much of the porosity in the samples comprising

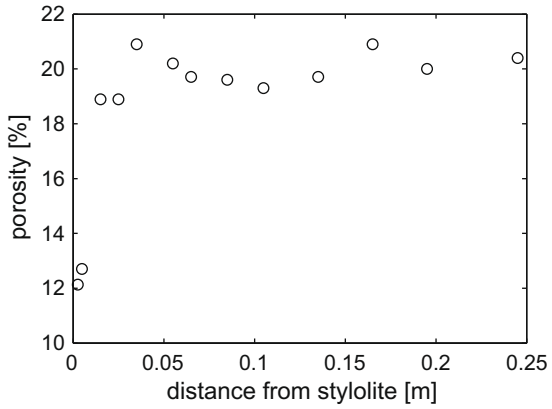

Fig. 4. Measured total porosity as a function of distance from stylolite interface in the Stø Formation sandstone.

pores 10–100 μm in diameter. Imaging also indicates that quartz mineralization in the Stø Formation typically takes the form of euhedral and subhedral overgrowths which intrude into large intergranular voids (Figs. 5 and 6). While the pore in the center of Fig. 5f (approximately 30–40 μm in diameter) exhibits euhedral overgrowths, euhedral crystal faces are not observed in the much smaller scale intragranular porosity (<5 μm) present in the same image. We consider it unlikely that these very small pores are artifacts of the sample preparation procedure.

The pore size distribution data provide additional quantitative information concerning the mineralization process. For all the samples, pores <10 μm in size consistently contribute a cumulative porosity of ~2.5–3%; by contrast the cumulative porosity for larger pores (>10 μm) varies from around 9% in the most mineralized samples (Fig. 7a–c) to approximately 18% in samples farthest from the stylolite (Fig. 7d–f). This critical observation suggests that pores >10 μm in size are filled during mineralization, while smaller pores (i.e., <10 μm) remain virtually unchanged.

While mineralization leads to a significant reduction in porosity, an examination of the cumulative surface area curves reveals that the total surface area in the mineralized samples is only slightly lower than in samples far from the stylolite (~0.039 and ~0.049 $m^2\ g^{-1}$, respectively; Fig. 8). This reflects the fact that in most cases more than 70% of the surface area in the Stø sandstone is associated with pores smaller than 10 μm. As we will discuss in the next section, this is likely to have important consequences for the application of kinetic models to geological systems.

3.2. Comparison of kinetic models

Importantly for the evaluation of interfacial energy effects, a comparison of the pore size distribution curves with the constant solubility and pore size dependent models (blue and red lines, respectively, in Fig. 9) highlights marked differences. At high levels of mineralization (Fig. 9a–c), the constant solubility model significantly overestimates the level of mineralization in micron-scale pores; in fact, irrespective of the parameter values, the model consistently predicts that voids smaller than ~10 μm should be completely filled in the region closest to the stylolite interface. By contrast, when the effect of surface energy on solubility is taken into account, mineralization of the smallest pores is inhibited and pore size patterns match very closely the measured curves. We emphasize here that while the parameter values play an important role in determining the evolution of porosity in both models, no combination of parameters was able to inhibit precipitation in the micron-scale pores of the constant solubility simulations. Moreover, we emphasize that in both models only three parameters (Pe, κ, and duration of the simulation) were varied to obtain the fits, and it is striking that the application of a new rate expression (Eq. (23)), in conjunction with the literature value for interfacial energy in the quartz-water system, achieves such a good agreement with the data.

Given that only large pores are filled in the pore size dependent model, we might expect to see an increase in the pore population at around 10 μm. In fact, close inspection of the model does reveal a slight rise in this region of ~0.1% in the pore space. The small magnitude of the increase can be explained by considering the much lower number per unit volume of larger pores (measured by L_d, defined in the model as $\phi_d/d^2(1-\frac{\omega-\sin\omega\cos\omega}{\sin^2\omega})$). While pore size is allowed to change, L_d for a given population of pores is kept constant; thus, if mineralization causes 100 μm pores with a partial porosity of 10% to shrink to 10 μm in size, only 0.1% will be added to the partial porosity of the original 10 μm size population. As this value falls well within the range of the porosity heterogeneity expected for rock samples, such a small effect is unlikely to be discernable with standard techniques.

Although the optimized model parameters must be interpreted with caution due to non-uniqueness limitations, we note that the optimization of constant solubility and pore size dependent solubility models yields overall similar values: $Pe = 1.93 \times 10^{-8}$, $\kappa = 3.31 \times 10^{6}$, and $\bar{t} = 0.0061$ for the constant solubility model, and $Pe = 2.31 \times 10^{-8}$, $\kappa = 3.14 \times 10^{6}$, and $\bar{t} = 0.0064$ for the pore size dependent model. Assuming an effective diffusion coefficient of 10^{-9} $m^2\ s^{-1}$, rescaling the dimensionless times using the relationship $t = \bar{t}H^2/(PeD_e)$ yields values of 6.3×10^5 years for the constant solubility model and 5.5×10^5 years for the pore size dependent model, respectively. However, these time scales for mineral precipitation cannot be compared directly due to the different levels of bulk supersaturation (S/S_0) generated in the two models; bulk supersaturation in the simulations is controlled both by Pe, which effectively determines the flux of solute into the porous domain, and the rapidity with which the dissolved mineral reprecipitates. An average value of $S/S_0 = 1.0005$ was computed for the pore size dependent model in the region nearest the stylolite; by contrast, a lower value of $S/S_0 = 1.0001$ was calculated for the constant solubility model. Although both values are within the range expected for diagenetic systems (Aase et al., 1996; Oelkers et al., 1996), they indicate that when interfacial energy effects are considered a significantly higher level of bulk saturation is required to achieve a comparable bulk reaction rate to that of the standard model.

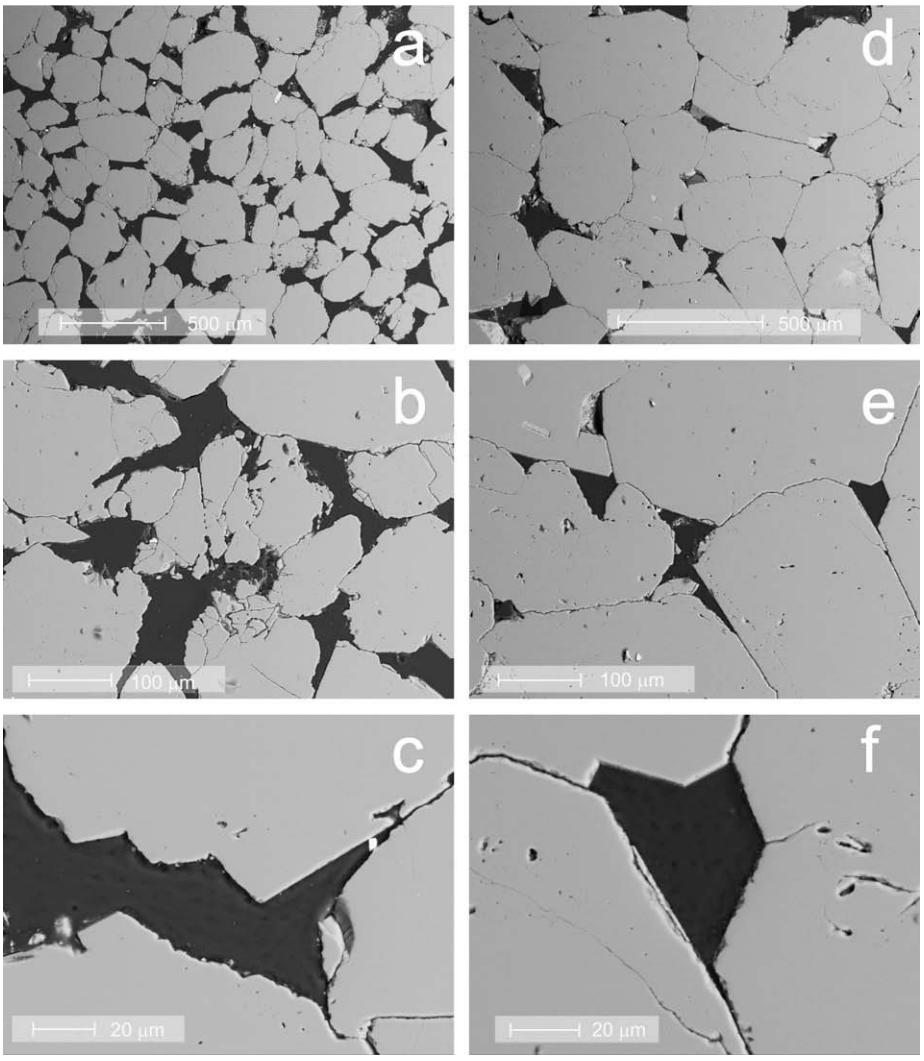

Fig. 5. Backstattered electron (BSE) images of polished sandstone at different magnifications sampled from (a)–(c) 24–25 cm and (d)–(f) 0–1 cm from the stylolite. Visual inspection indicates that most of the pore space comprises voids 10–100 μm in diameter. The medium gray regions are quartz while the dark gray zones are epoxy filling in the pores. Euhedral overgrowths can clearly be seen in (c) and (f). Digital image analysis reveals that the porosity is approximately 19.7% in the sample farthest from the stylolite and around 7.7% in the nearest sample. In these images there is a complete absence of clay minerals.

4. DISCUSSION

4.1. Additional mechanisms

The excellent agreement between our model and the pore size distribution data strongly suggests that interfacial effects are responsible for the preservation of micron-scale porosity in the mineralized samples. However, alternative mechanisms might produce similar effects. Clusters of clay minerals and clay coatings on quartz grains could affect quartz precipitation and act to inhibit mineral precipitation (Heald and Larese, 1974; McBride, 1989; Walderhaug et al., 2006; Aharonov and Katsman, 2009); however, the proportion of clay in the sandstone formation is extremely low, comprising only ~0.2% by volume (Walderhaug and Bjørkum, 2003), and it seems unlikely that such a small amount of material could account for the magnitude of porosity preservation measured in the present study. Moreover, BSE images show that clay minerals are absent from most of the small pores between the quartz grains (Fig. 5).

The creation of small pores during mineralization could also help to preserve micron-scale porosity. Some SEM images show that as quartz overgrowths intrude into intergranular voids, micropores form between the crystals. However, in order to reproduce the measured pore size distributions, the formation of new micron-scale porosity would have to balance almost exactly the amount of primary micron-scale porosity filled during each stage of mineralization, a result which would be most providential. In addition, visual inspection of the BSE and SEM images suggests that the phenomenon makes only a minor contribution to the overall porosity in the Stø Formation samples; for example, Figs. 5 and 6 show little of the highly porous intergranular cement sometimes seen in other rocks (Fig. 1).

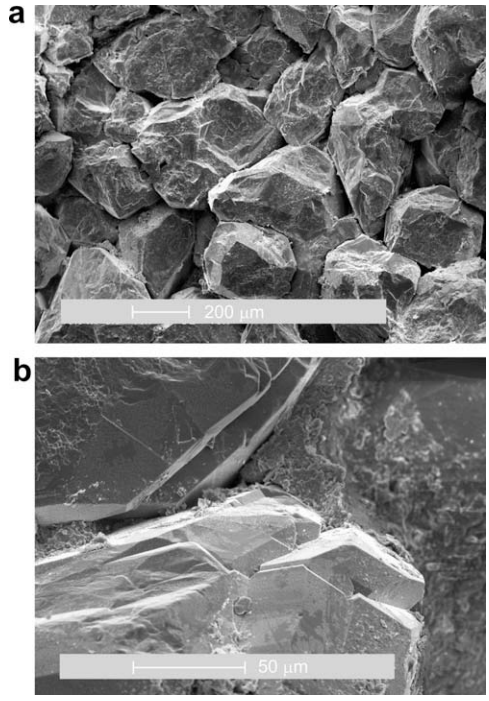

Fig. 6. SEM images of the unpolished sandstone in the interval 0–0.5 cm from the stylolite at (a) low magnification, and (b) high magnification. Note the euhedral to subhedral quartz overgrowths in the intergranular voids.

The lack of quartz precipitation in micron-scale voids could also be related to the reduced solute flux through small pores. Such a mechanism is expected to be important in systems in which (i) solute transport through the entire system is dominated by advection and (ii) reaction rates are rapid enough to be limited by the rate of mass transfer. However, in the diagenetic scenario examined here, diffusion rather than advection is likely to have been the primary mass transport process, and quartz precipitation is usually considered to be a very slow process occurring over thousands to millions of years. While completely isolated voids would preclude even diffusive mass transport, the fact that the submicron-scale pores are penetrated during the porosimetry measurements suggests that the porosity on different scales is connected, and diffusive mass transport should have been a pervasive mode of solute transfer during diagenesis. While it remains possible that the small pores were not wetted during the mineralization process, wetting behavior increases significantly at elevated fluid pressures and in the presence of dissolved salts (Zhang and Austad, 2006; Yu et al., 2009) and submicron-scale pores in the Stø Formation are likely to have contained fluid.

An additional mechanism – not taken into account in the model and which may also impact pore size distributions – is dissolution at individual grain contacts in the rock matrix adjacent to the stylolite. Although Walderhaug and Bjørkum (2003) reported that such dissolution was negligible, the irregular contacts between the grains observed in the BSE images may indicate that some degree of dissolu-

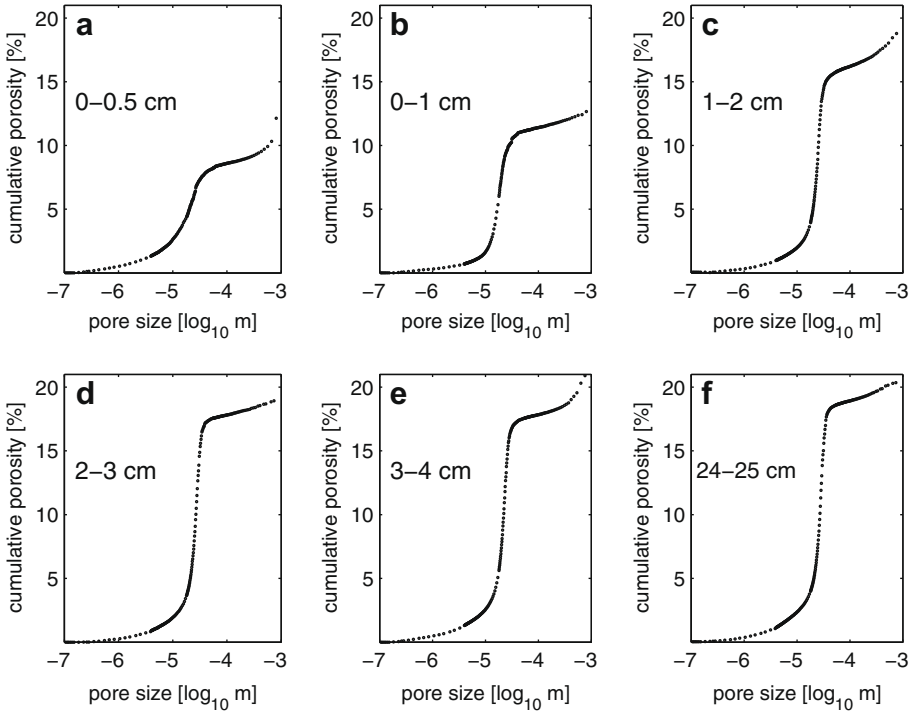

Fig. 7. Measured cumulative porosity curves at 6 distances from the stylolite: (a) 0–0.5 cm; (b) 0–1 cm; (c) 1–2 cm; (d) 2–3 cm; (e) 3–4 cm; and (f) 24–25 cm. Six additional samples at distances of 5–20 cm from the stylolite displayed only a low level of porosity reduction and very similar pore size distribution patterns to the sample farthest from the stylolite.

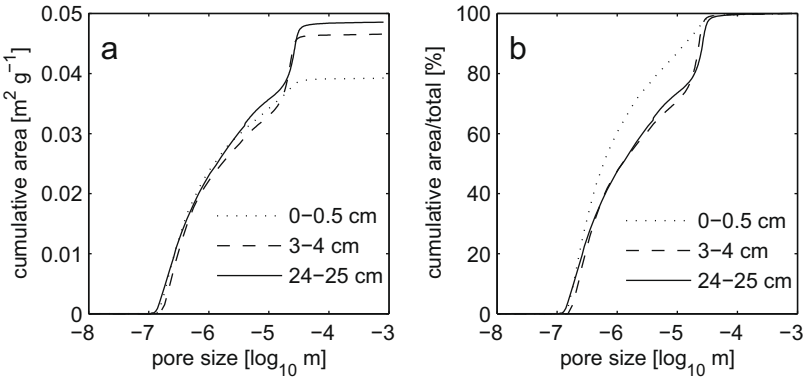

Fig. 8. Measured surface area curves at different distances from the stylolite. (a) Cumulative area as a function of pore size, and (b) cumulative area/total area as a function of pore size. Note that most of the surface area is associated with pores <10 μm in diameter, decreasing by less than 25% as a result of mineral precipitation.

tion does take place (Fig. 5). While the proportion of porosity reduction due to strain remains unclear, we note that intergranular dissolution should act simply to accelerate mineral precipitation and porosity reduction. Moreover, the conceptual model for the evolution of the porous medium does not need to change; pore size should respond to strain in the same way that it responds to mineral precipitation: squeezing the grains together will simply make pores smaller. Thus, strain on its own cannot account for the observed preservation of small pores.

The concept of crystal growth as a size dependent phenomenon is not new; in fact, the model presented here possesses some features common to Ostwald ripening, during which large crystals grow at the expense of smaller, more soluble crystals. While Steefel and Van Cappellen (1990) demonstrated that Ostwald ripening leads to changes in crystal size distributions, the study did not take into account the limitations imposed on crystal growth by the porous matrix. More recently, "textural equilibrium" models discussed in studies of metamorphic rock textures (e.g., Wark and Watson, 1998; Yoshino et al., 2006) have attempted to determine the effect of Ostwald ripening processes on pore shape and size, although the treatment takes an equilibrium approach, predicting only the final state of a system. In an effort to place the textural equilibrium theory within a kinetic framework, Holness and Siklos (2000) did however, conclude that the time scale required for pores to reach equilibrium is proportional to d^3, so that in a given system very tiny pores should reach equilibrium long before larger ones. The results here are consistent with such a prediction and might be interpreted as showing an evolving "active" porosity and a "stable" population of equilibrated pores. Our model, therefore, offers a truly dynamic approach to the evolution of crystal ripening within the confines of a preexisting porous structure.

Irrespective of the precise mechanism, the inhibition of mineral precipitation in small pores has important implications for mass transfer in diagenetic and metamorphic systems. As discussed by Emmanuel and Berkowitz (2007), clogging of the pore space in naturally mineralized systems is often thought to severely limit mass transfer; the results obtained here, however, indicate that micron-scale pores can remain open and connected, with diffusive and advective mass transfer potentially continuing indefinitely.

4.2. Implications for bulk reaction rates

In addition to demonstrating that the inhibition of mineral precipitation can occur in micron-scale pores, the model presented here also offers a straightforward way of quantifying the total effect of surface energy effects on reaction kinetics. Defining the critical pore diameter, d_{crit}, as the pore size below which mineral precipitation no longer occurs, the reduction in reaction rate can be approximated by the proportion of the total surface area associated with pores that are smaller than d_{crit}; from Eq. (17), d_{crit}, can be defined as

$$d_{\text{crit}} = \frac{1}{\ln(S/S_0)} \frac{4 v_m \gamma \sin\omega}{RT}. \tag{24}$$

Assuming $S/S_0 = 1.0005$, substitution of values for quartz and the measured temperature in the Stø Formation (Table 1) yields $d_{\text{crit}} = 8.2$ μm, and pores smaller than this value typically account for around 70% of the total surface area (Fig. 8), which will also correspond approximately to the level of reduction in the reaction rate.

Although the analysis here examines mineralization near stylolites, pore size should play a critical role in controlling reaction rates in a host of geological processes. Moreover, using Eq. (24), the pore size below which mineral precipitation ceases can be defined for any system in terms of two parameters: (1) the bulk supersaturation index, S/S_0, and (ii) the parameter Λ, which serves as a measure of the interfacial energy effect; in our simulations Λ is defined as $\Lambda = 4 v_m \gamma \sin\omega / RT$. In many rock forming processes, bulk supersaturation is expected to be low (< 1.01; Aase et al., 1996; Oelkers et al., 1996). In addition, assuming temperatures > 273 K during diagenesis and γ in the range 0–1.6 Jm^{-2} (Stumm and Morgan, 1996), substitution of parameter values into the definition of Λ yields $0 < \Lambda < 2 \times 10^{-8}$ m (from the values in Table 1, in the present study $\Lambda = 4.1 \times 10^{-9}$ m). Thus, for the range of typical values encountered in geological systems, d_{crit} will be greater than 1 μm (Fig. 10). Critically, in ubiquitous clastic and biogenic sedimentary rocks, including sandstone, limestone,

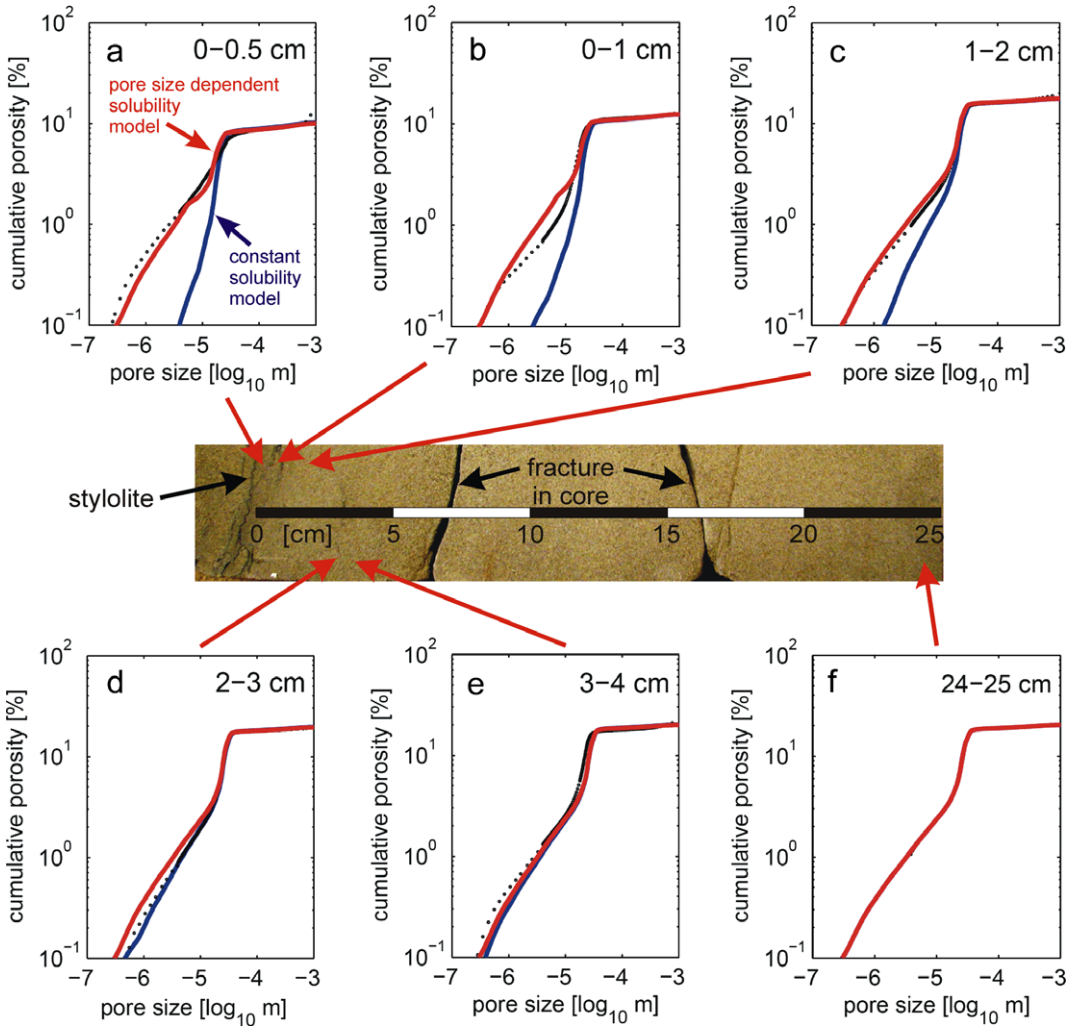

Fig. 9. Measured and simulated cumulative porosity curves at 6 distances from the stylolite: (a) 0–0.5 cm; (b) 0–1 cm; (c) 1–2 cm; (d) 2–3 cm; (e) 3–4 cm; and (f) 24–25 cm. Measured porosity (black circles) and model curves (blue – constant solubility model, red – pore size dependent solubility model) are given as a function of pore diameter. In (a)–(c), the pore size dependent solubility model is in excellent agreement with the measured data, while the constant solubility model overestimates the degree of mineralization in <10 μm pores. The position of the sample in the core is indicated in the photographic image. The cutoff at 10^{-3} m reflects the upper limit of the pore size measurements. The slightly darker area near the stylolite is due to cementation, rather than an increase in the abundance of clays. (For interpretation of the references to colour in this figure legend, the reader is referred to the web version of this article.)

chalk, and shale, it is not uncommon for $< 1\%$ of the total surface area to be associated with pores larger than 1 μm and $> 99\%$ to be associated with smaller pores (Fig. 11); this suggests that reactive surface areas, and hence overall reaction rates, could be reduced by 2 or more orders of magnitude by pore size effects.

Numerous studies have observed that kinetic rates of mineral reactions determined from field-based methods are often far lower than those measured in laboratory experiments (Blum and Stillings, 1995; Baxter and DePaolo, 2000; Oelkers et al., 2000; Yokoyama and Banfield, 2002; Baxter, 2003; Yoo and Mudd, 2008). Several mechanisms have been proposed to explain this inconsistency, including changes in surface area during reaction, depletion of reactive surfaces, and the buildup of leached layers and secondary precipitates (White and Brantley, 2003; Maher et al., 2006). It is possible, however, that for mineral precipitation rates a large part of the discrepancy could be a direct result of conducting laboratory experiments at levels of supersaturation that are much greater than those found in many geological systems. At elevated degrees of supersaturation, d_{crit} will become small enough to enable mineral precipitation on most of the available surfaces; consequently, rate constants in laboratory experiments will appear to be larger than those in natural systems. We emphasize that the level of rate reduction predicted for micron scale inhibition is sufficient to account for much of the anomaly, and the reduction in reaction rates due to interfacial energy effects in micron and nano-scale pores may be a major contributor to the apparent discrepancy.

Although the kinetics of mineral dissolution – particularly during weathering – is inherently more complex than the case of monomineralic mineral precipitation explored here, similar pore size related mechanisms could still play

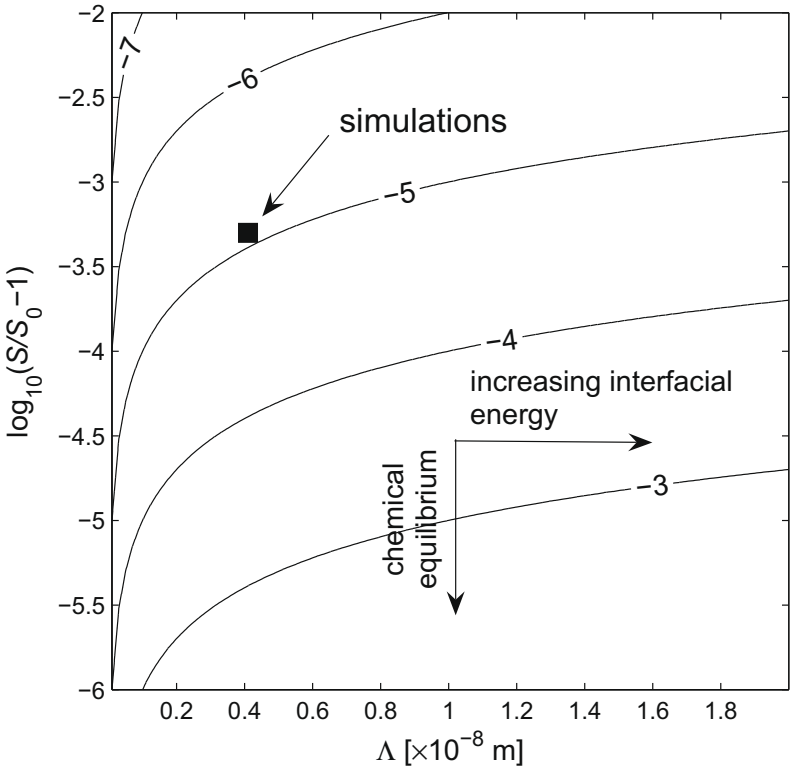

Fig. 10. Contours of critical pore size (d_{crit}; pore size below which mineral precipitation no longer occurs) as a function of Λ and the bulk supersaturation index (S/S_0). Contour values are in units of $\log_{10}$ m. Increasing values of Λ correspond to higher interfacial energy, while higher values on the y-axis reflect higher degrees of supersaturation, or increasing distance from equilibrium. As chemical equilibrium is approached, precipitation can be inhibited even in relatively large pores in systems with large Λ values, and for most of the range of parameters expected in geological systems d_{crit} will be greater than 1 μm. The mean bulk saturation and the value of Λ for quartz in the simulations is indicated by the black square, calculated from the literature values in Table 1.

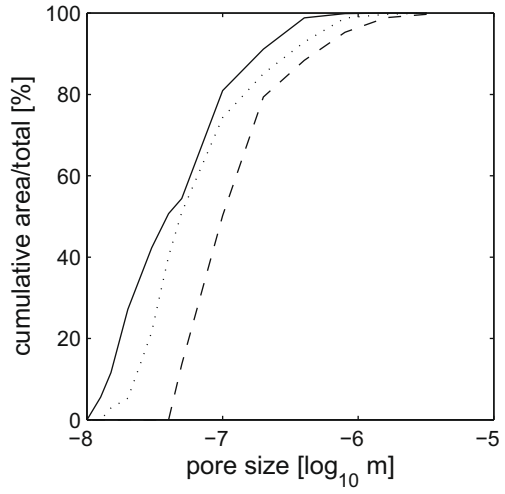

Fig. 11. Cumulative surface area/total area curves for representative fine-grained sandstones. In two of the samples > 99% of the total surface area is associated with pores in the submicron range. Data reported by (Kate and Gokhale, 2008).

an important role in determining reaction rates. During incongruent dissolution – which often occurs during weathering – rates of primary mineral dissolution are strongly correlated to rates of secondary mineral precipitation (Lasaga, 1998; Ganor et al., 2007; Maher et al., 2009; Zhu and Lu, 2009); thus a reduction in the rate of mineral precipitation due to interfacial energy effects could also slow overall weathering rates. More work, however, is required to explore the role played by interfacial energy during dissolution.

5. CONCLUDING REMARKS

In the present study, we present new measurements of pore size distributions in sandstone exhibiting varying levels of quartz mineralization. The results indicate that mineral precipitation does not occur in pores <10 μm. In addition, we use a reaction transport model to simulate the effect of mineral precipitation on porosity and pore size distributions. The simulations show that "standard" kinetic models predict that small pores should be entirely filled; by contrast, when the influence of surface energy in very small pores is included (pore size dependent model), mineralization is inhibited in small pores and excellent agreement with the data is obtained.

While the interfacial energy model is successful in reproducing the pore size patterns, the model clearly possesses a number of limitations: the present treatment is restricted to simple mono-mineralic systems and the effect

of intergranular dissolution is not accounted for. In addition, the pore geometry is highly idealized and does not truly reflect the complexity of natural porous media. Including such effects in kinetic models remains an ongoing challenge.

Whether or not the mechanism that leads to the inhibition of mineralization in the micron-scale pores of the Stø sandstone is ultimately related to interfacial energy effects or some other mechanism, the implications for the evaluation of bulk kinetic rates are great. In current models of reaction in porous geological media, total surface areas are often assumed to directly reflect the surface area available for reaction; as most of the surface area in rocks and soils is associated with pores <10 μm in size, the lack of precipitation in such pores is likely to mean that rates of reaction could be orders of magnitude lower than expected. Thus, our results suggest that current models of reactive transport in porous media – often used to evaluate changes in both the physical and chemical properties of the matrix – may need to be re-evaluated.

ACKNOWLEDGMENTS

The authors thank the Associate Editor E.H. Oelkers, C. Hilgers, and two anonymous reviewers for their thoughtful comments and suggestions. SE was generously supported by a Bateman Postdoctoral Fellowship from Yale University. We also thank J.O. Eckert for help with the BSE imaging and Z. Zhang for help with the SEM imaging. Acknowledgment is made to the Donors of the American Chemical Society Petroleum Research Fund for support of this research.

REFERENCES

Aase N. A., Bjørkum P. A. and Nadeau P. H. (1996) The effect of grain-coating microquartz on preservation of reservoir porosity. *Am. Assoc. Petrol. Geol. Bull.* **80**, 1654–1673.

Adamson A. W. (1990) *Physical Chemistry of Surfaces*, 5th ed. Wiley.

Aharonov E. and Katsman R. (2009) Interaction between pressure solution and clays in stylolite development: insights from modeling. *Am. J. Sci.* **309**, 607–632.

Baxter, E.F., 2003. Geochronology – linking the isotopic record with petrology and textures, vol. 220. Geological Society of London, Special Publication, Ch. Natural Constraints on Metamorphic Reaction Rates, pp. 183–202.

Baxter E. F. and DePaolo D. J. (2000) Field measurement of slow metamorphic reaction rates at temperatures of 500–600 °C. *Science* **288**, 1411–1414.

Bear J. (1972) *Dynamics of Fluids in Porous Media*. American Elsevier Publishing Company.

Berner R. A. (1980) *Early Diagenesis: A Theoretical Approach*. Princeton University Press, Princeton, New Jersey.

Blum A. and Stillings L. (1995) *Chemical Weathering Rates of Silicate Minerals*. , pp. 291–351.

Bryant S. (1995) Prediction of elastic-wave velocities in sandstones using structural models. *Geophysics* **60**, 437–446.

Emmanuel S. and Ague J. J. (2009) Modeling the impact of nanopores on mineralization in sedimentary rocks. *Water Resour. Res.* **45**, W04406.

Emmanuel S. and Berkowitz B. (2007) Effects of pore-size controlled solubility on reactive transport in heterogeneous rock. *Geophys. Res. Lett.* **34**, L06404.

Ganor J., Lu P., Zheng A. and Zhu C. (2007) Bridging the gap between laboratory measurements and field estimations of silicate weathering using simple calculations. *Environ. Geol.* **53**, 599–610.

Giesche H. (2006) Mercury porosimetry: a general (practical) overview. *Part. Part. Syst. Charact.* **23**, 9–19.

Heald M. T. and Larese R. E. (1974) Influence of coatings on quartz cementation. *J. Sediment. Res.* **44**, 1269–1274.

Holness M. B. and Siklos S. T. C. (2000) The rates and extent of textural equilibration in high-temperature fluid-bearing systems. *Chem. Geol.* **162**, 137–153.

Kang Q., Lichtner P. C. and Zhang D. (2006) Lattice Boltzmann pore-scale model for multicomponent reactive transport in porous media. *J. Geophys. Res.* **111**, B05203. doi:10.1029/2005JB003951.

Kang Q., Zhang D. and Chen S. (2003) Simulation of dissolution and precipitation in porous media. *J. Geophys. Res.* **108**, B102505.

Kate J. M. and Gokhale C. S. (2008) A simple method to estimate complete pore size distribution of rocks. *Eng. Geol.* **84**, 48–69.

Lasaga A. C. (1998) *Kinetic Theory in the Earth Sciences*. Princeton University Press, Princeton, New Jersey.

Lasaga A. C. and Rye D. M. (1993) Fluid flow and chemical reaction kinetics in metamorphic systems. *Am. J. Sci.* **293**, 361–404.

Lide D. R. (1996) *CRC Handbook of Chemistry and Physics*, 77th ed. CRC Press.

Maher K., Steefel C. I., DePaolo D. J. and Viani B. E. (2006) The mineral dissolution rate conundrum: Insights from reactive transport modeling of U isotopes and pore fluid chemistry in marine sediments. *Geochim. Cosmochim. Acta* **70**, 337–636.

Maher K., Steefel C. I., Stonestrom D. A. and White A. F. (2009) The role of secondary minerals and reaction affinity in regulating weathering rates at the Santa Cruz marine terrace chronosequence. *Geochim. Cosmochim. Acta* **73**, 2804–2831.

Mapstone M. B. (1975) Diagenetic history of North Sea chalk. *Sedimentology* **22**, 601–614.

McBride E. F. (1989) Quartz cement in sandstones: a review. *Earth Sci. Rev.* **26**, 69–112.

McHale J. M., Auroux A., Perrotta A. J. and Navrotsky A. (1997) Surface energies and thermodynamic phase stability in nanocrystalline aluminas. *Science* **277**, 788–791.

Navrotsky A., Mazeina L. and Majzlan J. (2008) Size-driven structural and thermodynamic complexity in iron oxides. *Science* **319**, 1635–1638.

Oelkers E. H., Bjørkum P. A. and Murphy W. M. (1996) A petrographic and computational investigation of quartz cementation and porosity reduction in North Sea sandstones. *Am. J. Sci.* **296**, 420–452.

Oelkers E. H., Bjørkum P. A., Walderhaug O., Nadeau P. H. and Murphy W. M. (2000) Making diagenesis obey thermodynamics and kinetics: the case of quartz cementation in sandstones from offshore mid-Norway. *Appl. Geochem.* **15**, 295–309.

Parks G. A. (1984) Surface and interfacial free energies of quartz. *J. Geophys. Res.* **89**, 3997–4008.

Putnis A. and Mauthe G. (2001) The effect of pore size on cementation in porous rocks. *Geofluids* **1**, 37–41.

Putnis A., Prieto M. and Fernandez-Diaz L. (1995) Supersaturation and crystallisation in porous media. *Geol. Mag.* **132**, 1–13.

Rijniers L. A., Huinink H. P., Pel L. and Kopinga K. (2005) Experimental evidence of crystallization pressure inside porous media. *Phys. Rev. Lett.* **94**, 075503.

Scherer G. W. (2004) Stress from crystallization of salt. *Cement Concrete Res.* **34**, 1613–1624.

Steefel P. and Van Cappellen P. (1990) A new kinetic approach to modelling waterrock interaction: the role of nucleation, pre-

cursors and Ostwald Ripening. *Geochim. Cosmochim. Acta* **54**, 2657–2677.

Stumm W. and Morgan J. J. (1996) *Aquatic Chemistry*, 3rd ed. Wiley Interscience.

Sullivan K. B. and McBride E. F. (1991) Diagenesis of sandstones at shale contacts and diagenetic heterogeneity, Frio Formation, Texas. *Am. Assoc. Petrol. Geol. Bull.* **75**, 121–138.

Tartakovsky A. M., Meakin P., Scheibe T. and Wood B. (2007) A smoothed particle hydrodynamics model for reactive transport and mineral precipitation in porous and fractured porous media. *Water Resour. Res.* **43**, W05437.

Uchida T. (1987) Pore-size distributions and the evaluation of permeability in reservoir rocks a proposal of empirical expressions with regard to petrological properties of pores. *J. Jpn. Assoc. Petrol. Technol.* **52**, 1–11.

Walderhaug O. and Bjørkum P. A. (2003) The effect of stylolite spacing on quartz cementation in the Lower Jurassic Stø Formation, Southern Barents Sea. *J. Sediment. Res.* **73**, 146–156.

Walderhaug O., Bjørkum P. A. and Aase N. E. (2006) Kaolin-coating of stylolites, effect on quartz cementation and general implications for dissolution at mineral interfaces. *J. Sediment. Res.* **76**, 234–243.

Wark D. A. and Watson E. B. (1998) Grain-scale permeabilities of texturally equilibrated, monomineralic rocks. *Earth Planet. Sci. Lett.* **164**, 591–605.

Washburn E. W. (1921) The dynamics of capillary flow. *Phys. Rev.* **17**, 273–283.

Wettlaufer J. S. (1999) Ice surfaces: macroscopic effects of microscopic structure. *Philos. Trans. R. Soc. A* **357**, 3403–3425.

White A. F. and Brantley S. L. (2003) The effect of time on the weathering of silicate minerals: Why do weathering rates differ in the laboratory and field? *Chem. Geol.* **202**, 479–506.

Wong P. K. and Oldershaw A. (1981) Burial cementation in the Devonian, Kaybob reef complex, Alberta, Canada. *J. Sediment. Petrol.* **73**, 507–520.

Yokoyama T. and Banfield J. F. (2002) Direct determinations of the rates of rhyolite dissolution and clay formation over 52,000 years and comparison with laboratory measurements. *Geochim. Cosmochim. Acta* **66**, 2665–2681.

Yoo K. and Mudd S. M. (2008) Discrepancy between mineral residence time and soil age: implications for the interpretation of chemical weathering rates. *Geology* **36**, 35–38.

Yoshino T., Price J. D., Wark D. A. and Watson E. B. (2006) Effect of faceting on pore geometry in texturally equilibrated rocks: implications for low permeability at low porosity. *Contrib. Mineral. Petrol.* **152**, 169–186.

Yu L., Evje S., Kleppe S., Karstad T., Fjelde I. and Skjaeveland S. M. (2009) Spontaneous imbibition of seawater into preferentially oil-wet chalk cores – experiments and simulations. *J. Petrol. Sci. Eng.* **66**, 171–179.

Zhang P. and Austad T. (2006) Wettability and oil recovery from carbonates: effects of temperature and potential determining ions. *Colloids Surf. A Physicochem. Eng. Asp.* **279**, 179–187.

Zhu C. (2005) Feldspar dissolution in saturated aquifers: in situ rates. *Geochim. Cosmochim. Acta* **69**, 1435–1453.

Zhu C. and Lu P. (2009) Alkali feldspar dissolution and secondary mineral precipitation in batch systems: 3. Saturation states of product minerals and reaction paths. *Geochim. Cosmochim. Acta* **73**, 3171–3200.

Associate editor: Eric H. Oelkers